Measurement of Solvation Responses at Multiple Sites in a Globular Protein

Paul Abbyad,[†] Xinghua Shi,[†] William Childs,[†] Tim B. McAnaney,[†] Bruce E. Cohen,[‡] and Steven G. Boxer*,[†]

Department of Chemistry, Stanford University, Stanford, California 94305-5080, and Biological Nanostructures Facility, The Molecular Foundry, Lawrence Berkeley National Laboratory, Berkeley, California 94720

Received: February 1, 2007; In Final Form: April 27, 2007

Proteins respond to electrostatic perturbations through complex reorganizations of their charged and polar groups, as well as those of the surrounding media. These solvation responses occur both in the protein interior and on its surface, though the exact mechanisms of solvation are not well understood, in part because of limited data on the solvation responses for any given protein. Here, we characterize the solvation kinetics at sites throughout the sequence of a small globular protein, the B1 domain of streptococcal protein G (GB1), using the synthetic fluorescent amino acid Aladan. Aladan was incorporated into seven different GB1 sites, and the time-dependent Stokes shift was measured over the femtosecond to nanosecond time scales by fluorescence upconversion and time-correlated single photon counting. The seven sites range from buried within the protein core to fully solvent-exposed on the protein surface, and are located on different protein secondary structures including β-sheets, helices, and loops. The dynamics in the protein sites were compared against the free fluorophore in buffer. All protein sites exhibited an initial, ultrafast Stokes shift on the subpicosecond time scale similar to that observed for the free fluorophore, but smaller in magnitude. As the probe is moved from the surface to more buried sites, the dynamics of the solvation response become slower, while no clear correlation between dynamics and secondary structure is observed. We suggest that restricted movements of the surrounding protein residues give rise to the observed long time dynamics and that such movements comprise a large portion of the protein's solvation response. The proper treatment of dynamic Stokes shift data when the time scale for solvation is comparable to the fluorescence lifetime is discussed.

Introduction

Electrostatic interactions affect nearly every aspect of protein structure and function[1,2] and play a major role in biological processes including electron[3,4] and proton transfer,[5] enzyme catalysis,[6] ligand binding,[7] and ion transport.[8] These processes, where charges often move over substantial distances, can be affected by both the time-averaged[9] and time-dependent variations in the electric field. Time-dependent variations derive from the dynamics of nearby charged, polar, and polarizable groups, as well as the mobility and accessibility of solvent molecules that lead to fluctuations in the electrostatic potential that can enhance specific solvation responses as charge develops. The fluctuations of electrostatic potential and more specific solvation responses depend upon this distribution of groups constrained by the overall structure of the protein scaffold. Compared to the solvation dynamics of simple fluid solvents (e.g., water and organic solvents), which are typically completed within the first few picoseconds,[10] the dynamics of a folded protein are more complex due to its tertiary structure and heterogeneity, and solvation occurs on many time scales.[11−15]

The experimental measurement of these dynamics or the solvation response of a protein to a charge perturbation is often achieved by monitoring the dynamic Stokes shift[16] of a fluorescent probe introduced into a unique site within the protein. The probe undergoes a substantial change in dipole moment upon excitation, creating a nonequilibrium environment for the surrounding protein. As the protein residues and nearby solvent molecules reorient to solvate the excited state of the probe, the emission spectrum shifts to lower energy with time and serves as a reporter for the extent of solvation. In order to be a useful probe of local protein solvation dynamics, the fluorophore must have fluorescence emission that is sensitive to the surrounding environment and must be targeted to a specific location within the protein. Studies of protein solvation have typically relied on the affinity of a dye for a particular ligand-binding site,[12,17−20] taken advantage of endogenous chromophores in the protein matrix,[21−23] or modified reactive side chains at the protein surface.[24] Tryptophan can also be used as a local probe of solvation dynamics and has recently been used to probe the protein hydration layer[25−27] or the protein core.[28] However, tryptophan's photophysics are complicated by the near degeneracy and differing polarities of its ^1L_a and ^1L_b excited states, which may limit its usefulness as a general probe.

6-Propionyl-2-(*N*,*N*-dimethylamino)naphthalene (PRODAN) has both electron donor and acceptor substituents that result in a large change in dipole moment upon excitation ($\Delta\mu$ determined to be between 4.4 and 5.0 D by Samanta et al.[29]) and exhibits a large solvatochromic fluorescence shift with increasing solvent polarity.[30] Experiments and calculations propose that in polar solvents PRODAN's emission is from a charge transfer state while at low temperatures or in nonpolar solvents the emission is from a locally excited state (LE).[31,32] There is still debate on whether the emitting charge transfer state is from a planar intermolecular charge transfer (PICT), a twisted intermolecular charge transfer (TICT), or a combination of both.[32−34] Since

* To whom correspondence should be addressed. Phone: (650) 723-4482. Fax: (650) 723-4817. E-mail: SBoxer@Stanford.edu.
[†] Stanford University.
[‡] Lawrence Berkeley National Laboratory.

10.1021/jp0709104 CCC: $37.00
Published on Web 06/26/2007

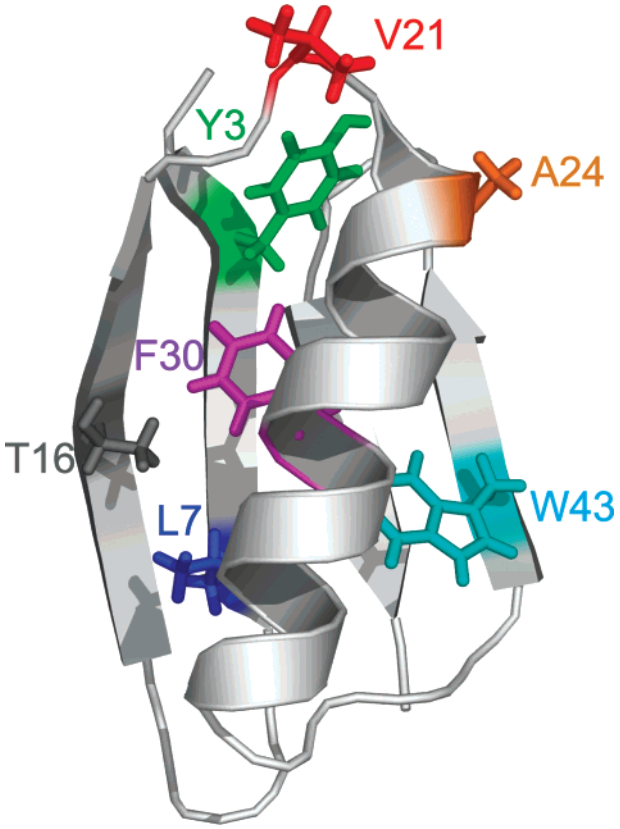

Figure 1. Sites of incorporation of fluorescent amino acid Aladan into the B1 domain of streptococcal protein G. The crystal structure is from ref 59 (Protein Data Bank 3GB1). The sites of incorporating were characterized as buried (F30, L7), partially exposed (W43, Y3), and fully exposed (A24, V21, T16).

CHART 1

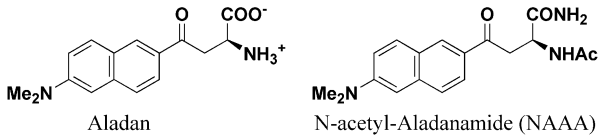

its initial synthesis, this chromophore and its derivatives have been widely utilized as probes of proteins,[35] lipids,[36] and cellular membranes.[37] PRODAN served as the inspiration for the synthetic fluorescent amino acid Aladan[11] (Chart 1). Aladan shares the same conjugated chromophore as PRODAN and shows similar solvatochromic fluorescence shifts.[11] As an amino acid, Aladan can be incorporated site-specifically throughout a given protein sequence, including the protein interior, permitting us to undertake a comprehensive characterization of protein solvation dynamics.

Aladan was incorporated into seven different sites of the B1 domain of streptococcal protein G (GB1; Figure 1) by solid-phase synthesis (see Materials and Methods). The sites were characterized as buried (F30, L7), partially exposed (W43, Y3), and primarily solvent exposed (A24, V21, T16).[11,38] The sites are also located on the different secondary structures of the protein including the β-sheets (L7, W43, Y3, T16), on the helix (F30, A24), and in a loop region (V21). Aladan's peak fluorescence at these sites (ranging from 468 to 525 nm) suggests that the emission is from a charge transfer state.[32]

Earlier time-resolved upconversion experiments (for Aladan at positions L7, F30, and W43) measured protein relaxation over 160 ps and demonstrated that the Aladan-substituted proteins experienced a rapid solvation response at early times with differences at longer time scales that depended on the probe location.[11] In this work, we present the solvation dynamics over the full lifetime of the Aladan probe, extend the measurements to four additional sites, and make comparisons with the dynamics of the free fluorophore in solution. This study represents the most comprehensive characterization of a protein's solvation response to date.

Materials and Methods

Protein Synthesis. Aladan was synthesized as previously described.[11] GB1 synthesis (amino acid sequence as in ref 11) was carried out by standard Fmoc/HBTU chemistry on Wang resin with an Applied Biosystems 433A Peptide Synthesizer, except that resin was moved from the synthesizer to a round-bottom flask for Aladan coupling, and Fmoc-Aladan was coupled to the sequence using HATU. Proteins were cleaved from the resin (5% thioanisole, 5% H_2O, and 1% TIPS in TFA) for 1 h, precipitated with ether, and centrifuged. The resulting pellet was washed with ether and quickly resuspended in 20 mL of 200 mM Tris buffer, pH 8.0. Low molecular weight impurities were removed with a Centricon spin dialysis column (3000 Da molecular weight cutoff; Millipore). Refolded protein was purified by chromatography on IgG-Sepharose (Amersham), washing exhaustively with PBS, pH 7.4, to remove unbound material, and eluting with acetate buffer, pH 3.4, until all yellow color had been washed from the column. Eluted fractions were frozen and lyophilized, and then purified by reverse-phase HPLC with a Vydac C18 column, using a shallow (0.1%/min) H_2O/CH_3CN gradient. Samples containing protein were frozen and lyophilized, and then resuspended in water and relyophilized to remove residual TFA. Purities and molecular masses were assayed with an LCQ MS/MS electrospray mass spectrometer (Thermo Finnigan).

Structural Characterization. All Aladan-GB1's showed similar affinity to ligand as wild type. Further characterization was performed on F30, L7, W43, and A24 to ensure that the Aladan does not disrupt the tertiary fold of GB1.[11] These sites exhibited cooperative and reversible two-state unfolding transitions, and distinct differences at buried and exposed sites in their accessibility to the hydrophilic collisional quencher iodide. ^{1}H NMR studies of GB1 with buried Aladan residues show the expected dispersed amide regions of well-packed globular proteins and include resonances characteristic of the wild-type protein interior.[39]

Sample Preparation and Steady-State Characterization. The seven Aladan-containing proteins (Figure 1) and *N*-acetyl-Aladanamide (NAAA) (see Chart 1) were dissolved to $A_{400} = 5$ in aqueous buffer (150 mM NaCl and 50 mM NaOAc, pH 5.4) as described previously.[11] The absorption spectrum of each sample was recorded on a Perkin-Elmer Lambda 2 UV/vis spectrophotometer (Perkin-Elmer, MA). Steady-state fluorescence spectra were recorded using a Spex Fluorolog fluorimeter with a Spex 1620 dual grating emission monochromator (HORIBA Jobin Yvon, Edison, NJ). Spectra were corrected for detection efficiency using a series of standards and technical emission spectra that covered the appropriate fluorescence range.[40]

Ultrafast Fluorescence Spectroscopy. The time-resolved fluorescence of Aladan-GB1's and NAAA in aqueous buffer was measured at 12 wavelengths by a fluorescence upconversion setup described previously[41−43] and by time-correlated single photon counting (TCSPC). The samples, stirred continuously in a 1 mm path length quartz cuvette, were excited at 82 MHz by a 400 nm excitation pulse generated from the second

harmonic of an argon ion pumped titanium:sapphire laser. To avoid fluorescence quenching and photodestruction by oxygen, the cuvettes were sealed and kept under an argon atmosphere. Samples typically had an absorption of $A_{400} = 0.3-0.6$ in the 1 mm path length cuvette. Steady-state fluorescence spectra were acquired before and after time-resolved experiments to ensure that samples did not deteriorate over the course of experiments.

For upconversion measurements, the instrument response function (IRF) generated from the mixing of the gate beam with scattered excitation light was typically ~160 fs full width at half-maximum (fwhm). A 200 mm ATS100 delay line (Aerotech, PA) in the excitation pathway afforded an extended time window of 1.33 ns compared to earlier upconversion measurements[11] and allowed for logarithmic time steps. The sample was excited with 5 mW of light (6 pJ/pulse) polarized at the magic angle with respect to the gate beam. A UG 11 filter provided good transmission of the upconverted light over the desired wavelength range while sufficiently blocking the nonupconverted fluorescence and residual, scattered 400 nm excitation light. Upconverted fluorescence was detected by a photon counting R928P PMT (Hamamatsu, Japan) attached to a 270M dual-port monochromator (Spex Industries, NJ).

For time-correlated single photon counting experiments, samples were excited by 1.6 mW of light (2 pJ/pulse) polarized at the magic angle with respect to a Glan-Thomson polarizer placed in the emission detection pathway. The IRF of the TCSPC setup, measured by detection of scattered excitation light, was ~30 ps fwhm, and the time window of data acquisition was ~10 ns with 12.2 ps/channel resolution. A 420 nm long-pass filter provided good transmission of the fluorescence emission and sufficiently blocked scattered excitation light. Fluorescence was detected through the second port of the monochromator by an R3809U-50 MCP (Hamamatsu) and an SPC-630 TCSPC module (Becker & Hickl, Germany). Anisotropy scans were acquired by rotating the polarization of the excitation beam with a 1/2-λ plate to parallel and perpendicular polarizations with respect to the polarizer. The time-resolved anisotropy was calculated as $r(t) = (I_{\parallel}(t) - I_{\perp}(t))/(I_{\parallel}(t) + 2I_{\perp}(t))$.

Data Analysis. The data sets acquired by the TCSPC technique were analyzed by fitting the data to the cyclic convolution of the IRF with a sum of exponentials (A_i, τ_i), a baseline B, and a time offset t_0:

$$I^{\mathrm{TCSPC}}(t;\lambda) = \mathrm{IRF} \otimes \sum \frac{A_i}{1 - \mathrm{e}^{-1/f\tau_i}} \mathrm{e}^{-(t-t_0)/\tau_i} + B \qquad (1)$$

where f is the repetition frequency of the laser pulses (82 MHz). The cyclic convolution and the denominator in the preexponential term account for the fluorescence that remains preceding excitation events and is important when the radiative rate of emission is comparable to the repetition rate of the laser (typical fluorescence lifetimes are 2−4 ns and the time between laser pulses is 12 ns). The upconversion data were fit to the analytical expression of a Gaussian-type IRF convolved with a sum of exponentials (A_j, τ_j), a baseline B, and a time offset t_0. The longer time components (> ~500 ps) and their relative amplitudes were kept fixed to those values obtained by TCSPC and were scaled by a single parameter C:

$$I^{\mathrm{UPC}}(t;\lambda) = \mathrm{IRF} \otimes [\sum A_j \mathrm{e}^{-(t-t_0)/\tau_j} + C\sum (A_i \mathrm{e}^{-(t-t_0)/\tau_i} + A_i \mathrm{e}^{-(t+1/f-t_0)/\tau_i})] + B \qquad (2)$$

The contribution from the previous pulse ($t_0 - 1/f$) was included for the longer time components. An analytical expression rather than a numerical convolution was used due to the nonlinear step size of data acquisition:

$$\mathrm{IRF} \otimes \mathrm{e}^{-(t-t_0)/\tau} = \frac{1}{2}(\mathrm{e}^{(\sigma^2\tau^2/2)-(t-t_0)/\tau})\left(1 + \mathrm{erf}\left(\frac{(t-t_0) - \sigma^2\tau}{\sqrt{2}\sigma}\right)\right) \qquad (3)$$

However, this simplification is justified since the IRF of the upconversion setup is well described by a simple Gaussian line shape with fwhm $= 2\sigma\sqrt{2\ln(2)}$. Overall, this fitting procedure creates a multiexponential decay series for each wavelength $D(t;\lambda)$ that seamlessly spans the time scale of the upconversion and TCSPC measurements.

The use of the decay series $D(t;\lambda)$ removes unwanted contributions from the IRF, background, fluorescence from previous pulses, and the group velocity mismatch present in the raw data. Although the decay series can be extrapolated to arbitrary short and long times, it was limited to the experimental time window of 80 fs−10 ns. Time-resolved emission spectra were obtained by normalizing the integrated areas of the decay series at each wavelength to their respective intensities in the steady-state fluorescence spectrum $F_{\mathrm{ss}}(\lambda)$ and converted to frequency representation:[10]

$$F(\nu;t) = \nu^2 \frac{D(t;\lambda)\, F_{\mathrm{ss}}(\lambda)}{\sum A_j\tau_j + C\sum A_i\tau_i} \qquad (4)$$

The dynamic Stokes shift, as characterized by the peak emission frequency $\nu_{\mathrm{p}}(t)$, was calculated by fitting the time-resolved spectra to a log-normal line shape and averaged over two or three independent data sets for each sample (with the exception of T16 where only a single date set was obtained due to limited sample) from 80 fs to 10 ns. This procedure produces a smooth curve of peak emission frequency over time and does not include the noise inherent in the experiment. At late times the peak frequency is less well-defined than at early times due to low overall fluorescence intensity.

To characterize the time scales of solvation in the dynamic Stokes shift data, a maximum entropy method (MEM) analysis was performed using the program MemExp v2.0 developed by Peter J. Steinbach of the NIH.[44,45] The MEM analysis strives to fit the dynamic Stokes shift with a distribution of lifetimes equally spaced in $\log(\tau)$ space while simultaneously maximizing the entropy term $S = \sum w_i \ln(w_i)$, where w_i is the weight of lifetime τ_i. The MEM solution gives the distribution of lifetimes that best fits the data and is the least structured. The relative importance given to each of these factors will affect the shape of the distribution, and the selection of an acceptable distribution is described in detail in ref 44.

MEM is sensitive to the error bounds of the data; however, the dynamic Stokes shift has no error since it is derived from the fits to the fluorescence decays. For the purpose of this analysis, a reasonable estimation of the error of the measurement must be included in the dynamic Stokes shift. This was done by adding Poisson-distributed noise appropriate to the count rate of the measurement to the decay series ($D(t;\lambda)$ in eq 4). From this modified decay series, time-resolved fluorescence spectra were constructed and fit to a log-normal line shape as described above. The resulting dynamic Stokes shift, which now includes simulated noise, was analyzed by MEM.

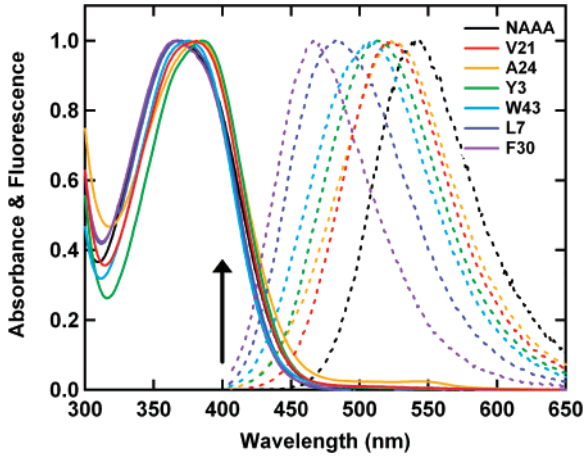

Figure 2. Normalized steady-state absorbance (solid) and fluorescence (dashed) spectra of Aladan at sites V21 (red), A24 (orange), Y3 (green), W43 (cyan), L7 (blue), and F30 (purple) in GB1 and NAAA in buffer (black). The excitation wavelength for steady-state and time-resolved fluorescence measurements, 400 nm, is indicated by the arrow. For clarity the spectra for T16 were omitted but they overlap very closely with the spectra of V21.

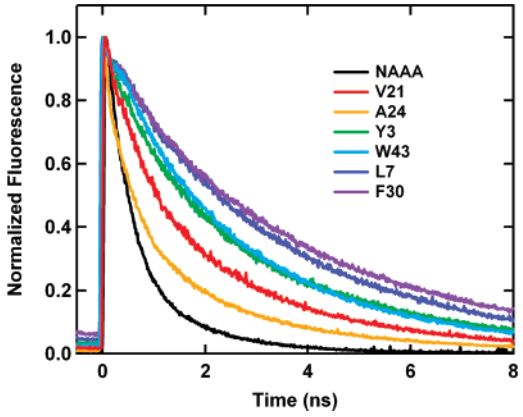

Figure 3. Normalized integrated fluorescence intensity of Aladan at sites V21 (red), A24 (orange), Y3 (green), W43 (cyan), L7 (blue), and F30 (purple) in GB1 and NAAA in buffer (black) measured by TCSPC following excitation at 400 nm. The integrated intensity was determined by fitting at each time point the time-resolved spectra to a log-nornal line shape. The fit parameters were then used to determine the integrated intensity of the curve.[10] The fluorescence at negative time is primarily emission from the previous excitation pulse. T16 is not included as the integrated fluorescence decay overlays very closely with that of V21.

Results and Discussion

Steady-State Spectroscopy. The steady-state absorption and fluorescence spectra of the Aladan-GB1 mutants and NAAA in buffer are shown in Figure 2. The NAAA emission maximum depends strongly on the polarity of the solvent,[11] showing a 545 nm peak in aqueous buffer following excitation at 400 nm. While the seven mutants exhibit only small differences in their absorption spectra, their emission spectra vary dramatically with peaks that range from 468 to 525 nm depending on the location of the probe within the protein (Figure 1). Mutants whose native residues were characterized as being buried within the protein core (F30 and L7) exhibit a smaller Stokes shift than those characterized as being partially (W43 and Y3) or fully (A24, V21, and T16) exposed to the surrounding solvent,[38] and none exhibit a Stokes shift as large as that observed for NAAA in buffer. Based on the native structure, residue T16 could be considered partially buried. However, upon replacement with the bulkier Aladan its emission properties closely resemble those of the solvent-exposed sites. Steric constraints likely push Aladan into the bulk solvent at this site, and T16 was operationally classified as solvent exposed.

Time-Resolved Fluorescence. For all samples studied, the time-resolved emission measured by fluorescence upconversion exhibits a rapid decay at shorter wavelengths and rising kinetics at longer wavelengths, evidence of relaxation from high- to low-energy emitting conformations. These kinetic signatures are a hallmark of the time-dependent Stokes shift that occurs as the surrounding protein and solvent reorient to solvate the charge-separated probe created following excitation. The decay of emission on the nanosecond time scale, measured by TCSPC, shows a correlation between the lifetime of the Aladan probe and the degree of solvent exposure (Figure 3). The kinetics measured at any discrete wavelength are affected by solvation processes that occur on a comparable time scale; therefore, the lifetime of the probe was determined by fitting the integrated intensity of the time-resolved spectra. The decay of emission intensity for NAAA in buffer is well fit with two lifetimes, (73%) 0.35 ns and (27%) 1.35 ns, which are similar to the biexponential decay times of 0.5 and 1.6−1.9 ns reported for PRODAN in water.[46,47] The emission decays for the seven Aladan-GB1 mutants are more complex, requiring at least three exponential components in all cases (Table 1). The mean lifetimes $\langle\tau_f\rangle = \sum A_i\tau_i$ for the buried sites are 2.8 ns for L7 and 3.2 ns for F30. Exposed sites such as T16, V21, and A24 have mean lifetimes of 1.5, 1.7, and 1.0 ns, respectively. The partially buried sites showed intermediate lifetimes of 2.3 ns for Y3 and 2.5 ns for W43. Thus the average fluorescent lifetime of the probe at the buried sites is longer than when exposed to solvent or free in solution. The increase in fluorescent quantum yield of PRODAN and its derivatives when bound to proteins is well documented[48−50] and is likely due to contributions from a reduced rate of collisional quenching by solvent molecules and possibly reduced conformational freedom of the amine or carbonyl groups due to the close packing of surrounding protein.

Time-Resolved Anisotropy. The time-resolved anisotropy of NAAA, as measured by TCSPC, shows an initial anisotropy $r(0)$ of 0.37 which rapidly decays to zero with the rotational correlation time of the probe, ~185 ps (Figure 4). As expected, the time-resolved anisotropies of the Aladan-GB1 mutants decay on a time scale much longer than that of the free fluorophore. The time-resolved anisotropies of the F30, L7, and W43 mutants are identical to within the error of the measurement. All three

TABLE 1: Fit Parameters for the Decay of Integrated Fluorescence Intensity Measured by TCSPC

sample	A_1 (%)	τ_1 (ns)	A_2 (%)	τ_2 (ns)	A_3 (%)	τ_2 (ns)
NAAA	27 ± 2	1.3 ± 0.03	73 ± 2	0.35 ± 0.02		
T16	42 ± 6	2.88 ± 0.02	38 ± 2	0.8 ± 0.1	20 ± 5	0.15 ± 0.03
V21	43 ± 6	3.0 ± 0.2	35 ± 4	1.0 ± 0.3	22 ± 10	0.35 ± 0.07
A24	23 ± 5	2.9 ± 0.4	39 ± 5	0.8 ± 0.3	38 ± 9	0.18 ± 0.08
Y3	48 ± 2	3.83 ± 0.01	32 ± 3	1.4 ± 0.1	19 ± 5	0.32 ± 0.09
W43	35 ± 6	4.1 ± 0.3	54 ± 4	1.9 ± 0.3	11 ± 2	0.3 ± 0.2
L7	72 ± 4	3.7 ± 0.1	15 ± 1	0.94 ± 0.19	13 ± 4	0.10 ± 0.04
F30	72 ± 5	4.2 ± 0.2	15 ± 1	1.1 ± 0.3	13 ± 4	0.21 ± 0.05

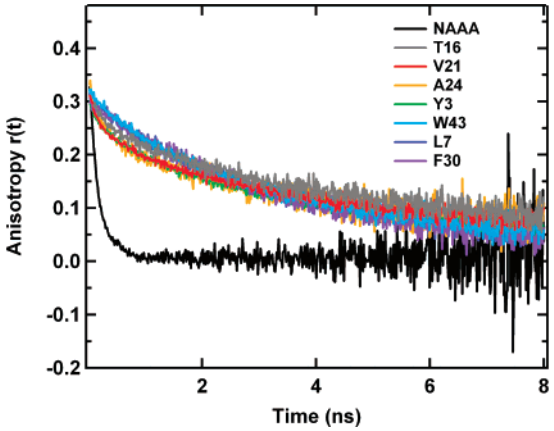

Figure 4. Time-resolved fluorescence anisotropy of Aladan at sites T16 (gray), V21 (red), A24 (orange), Y3 (green), W43 (cyan), L7 (blue), and F30 (purple) in GB1 and NAAA in buffer (black) measured by TCSPC following excitation at 400 nm.

mutants show high initial anisotropies ($r(0) > 0.31$) that decay with rotational correlation times of $\sim 2.5 \pm 0.3$ ns (65%) and 8.6 ± 1.5 ns (35%) consistent with the small size of the GB1 protein.[51] The A24, V21, and Y3 mutants have similar initial anisotropy following excitation, $r(0) = 0.35$; however, they then exhibit faster decay times of $\sim 0.6 \pm 0.2$ ns (41%) and 7.9 ± 0.3 ns (59%), indicating that they experience a greater degree of rotational freedom at the protein surface compared to their buried counterparts. The T16 mutant shows intermediate anisotropy behavior with decay times of 0.72 ± 0.03 ns (23%) and 8.9 ± 0.5 ns (77%). The time-resolved anisotropies suggest that solvation of the probe is not due to a significant reorientation of the probe, such as a redistribution of the probe from the protein core into the surrounding solvent following excitation. Such a specific, orientational response of the probe would cause a change in the anisotropy on a much faster time scale than that of global protein rotation. Furthermore, the relatively simple anisotropy decays suggest that the emitting state is the same as the initially excited state and that the Aladan probe does not undergo any complicated photophysics.

Solvation Dynamics of Aladan-GB1's. Time-resolved emission spectra were reconstructed from the upconversion and TCSPC kinetic traces, and the dynamic Stokes shift was characterized by the time-dependent shift of the peak emission frequency. Given the 160 fs IRF of the upconversion setup, it is difficult to accurately extrapolate time-resolved emission spectra at times < 80 fs; therefore, this was taken as the upper limit of time resolution. The dynamic Stokes shifts of seven Aladan mutants and the free probe NAAA are shown in Figure 5. The plot includes both individual data sets (dashed curves) and the average (solid curves) for each site. There is good reproducibility between data sets of the same site.

The Aladan mutants exhibit a diversity of solvation responses, in both magnitude and time scale. The starting frequency also differs substantially between different protein sites ranging from 22 460 cm^{-1} for the buried site F30 to 20 260 cm^{-1} for solvent-exposed T16. Qualitatively, the solvation dynamics at the most exposed sites A24, V21, and T16 more closely resemble those of the free probe in solution. In general, as the sites probed become more buried, the time scale of the response exhibits slower dynamics. Surprisingly, the time-resolved emission spectra of W43 and A24, and to a lesser extent V21, T16, and Y3, appear to blue-shift after ca. 1 ns.

The maximum shifts observed, excluding the blue shifts seen at longer times (discussed below), are ~ 2460 cm^{-1} for W43

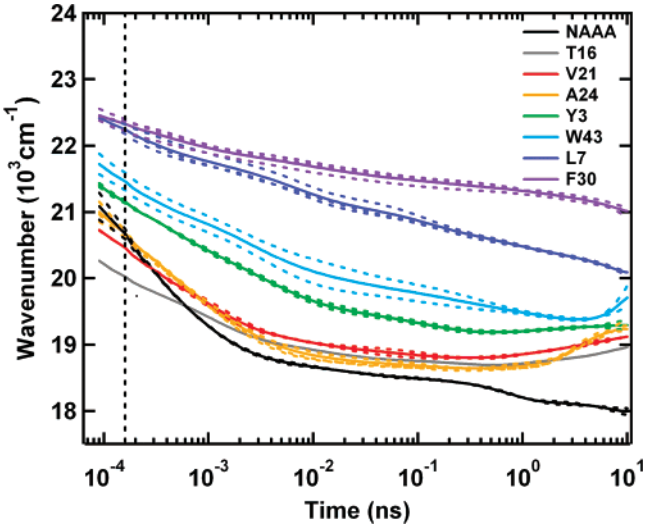

Figure 5. Dynamic Stokes shift, as characterized by the peak emission energy of the time-resolved emission spectra (see text), of Aladan at sites T16 (gray), V21 (red), A24 (orange), Y3 (green), W43 (cyan), L7 (blue), and F30 (purple) in GB1 and NAAA in buffer (black) measured by upconversion spectroscopy and TCSPC following excitation at 400 nm. Dashed curves are individual data sets, while the solid curve is the average for a site. The 160 fs IRF of the upconversion setup is indicated by a vertical dashed line.

and ~ 2220 cm^{-1} for Y3, the partially exposed sites. For the solvent-exposed sites T16, V21, and A24, the maximum shifts observed are ~ 1560, 1930, and 2500 cm^{-1}, respectively. The total observed shift of the peak emission frequency is ~ 1570 and 2370 cm^{-1} for the buried sites F30 and L7, respectively. The magnitude of these shifts likely underestimates the capacity of the protein to solvate charge at these sites because the measurement becomes limited by the excited-state lifetime of the probe. In simple solvents, the time scale of fluorescence (τ_f, typically approximately nanoseconds) is much longer than that of solvation (τ_s, typically 100 fs−10 ps), so steady-state emission originates primarily from the fully solvated state.[10] As the time scales τ_s and τ_f become comparable, as can be the case in protein systems (or in very viscous solvents and glasses), the ultimate capacity of the protein to solvate charge may never be realized within the excited-state lifetime of the probe. Therefore, the Stokes shifts observed in these experiments serve as lower limits of the site-specific dielectric capacity of the protein. This limited observation window also prevents the accurate construction of the solvation correlation function commonly used to characterize the response of simple solvents:

$$C(t) = \frac{\nu(t) - \nu(\infty)}{\nu(0) - \nu(\infty)} \tag{5}$$

Typically, the peak emission frequency observed at steady state is taken as $\nu(\infty)$; however, this is valid only when τ_f is much longer than τ_s, and is justified in the case of simple fluid solvents. When $\tau_f \approx \tau_s$, the steady-state emission spectrum no longer reflects the maximum solvation capacity of the solvent under investigation. The separation of time scales $\tau_f \gg \tau_s$ is not known a priori for protein systems, so we avoid the use of normalized correlation functions and instead report the absolute observed frequency shift over the specified time window.

The dynamic Stokes shifts of the seven mutants are not well described by a simple series of exponential decays; therefore, a maximum entropy method (MEM) analysis was performed to characterize the time scales of solvation. For the T16, V21, A24, Y3, and W43 mutants, the MEM analysis was restricted to the

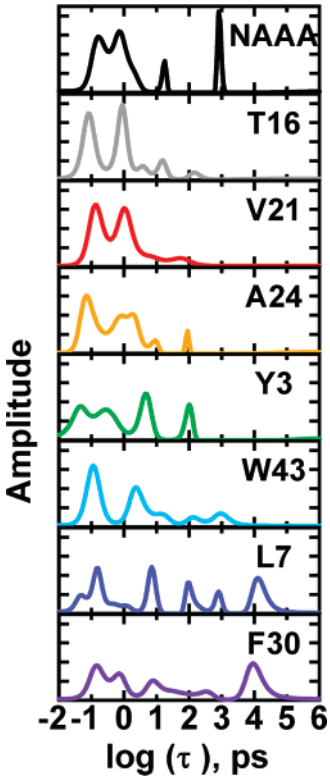

Figure 6. MEM analysis of the contributions to the dynamic Stokes shift of Aladan at sites T16 (gray), V21 (red), A24 (orange), Y3 (green), W43 (cyan), L7 (blue), and F30 (purple) in GB1 and NAAA in buffer (black).

red-shifting portion of the dynamic Stokes shift curve; the results for the seven Aladan-GB1 mutants are shown in Figure 6.

All of the sites examined appear capable of an ultrafast solvation response and exhibit peaks in the MEM distribution ranging from ~80 to 140 fs. These ultrafast components have been attributed to the inertial solvation response of bulk water[18,25,52] or of the protein.[17,23] The presence of longer time scale solvation responses becomes more pronounced for probes buried within the protein. The partially exposed sites, Y3 and W43, show peaks from 100 to 1000 ps while both buried probe mutants, F30 and L7, have significant peaks at time scales as long as ~10 ns, longer than the lifetime of the probe itself and near the end of our experimental observation window. These long time components are likely a result of global protein motions along the solvation coordinate and the restricted motions of nearby side chains and, possibly, solvent molecules located in the protein's hydration shell.[53] By comparison, the peaks for the solvent-exposed sites (A24, V21 and T16) are concentrated at early times (<100 ps). Recent simulations have predicted relaxation times of greater than 1 ns for position T16.[15] This long time component was not observed experimentally but it may be obscured by the blue shift at this site (see below). The solvent-exposed sites resemble the MEM distribution of NAAA that has two main peaks at 158 and 794 fs. These peaks comprise greater than 75% of the total solvation response, results consistent with the expected ultrafast solvation response of water.[54] NAAA also shows peaks at 18 and 790 ps, both of which are longer than relaxation components previously observed for small organic probes in water.[25,54] The magnitude of these components is relatively small and makes up less than 25% of the total solvation response. It has been shown that, at high concentrations, PRODAN forms soluble aggregates in water.[46] NAAA contains two hydrogen bond donors (the *N*-acetyl or acetamide nitrogens), as well as a hydrogen bond acceptor (the side chain carbonyl oxygen) that could promote intermolecular hydrogen bonding. A small population of associated NAAA molecules could explain the observed longer solvation components. These intermolecular interactions should be minimized when Aladan is incorporated in a protein and its hydrogen bond donors are part of the protein backbone.

There are no clear trends in dynamics for different secondary structures. Both sites V21 (on a loop) and A24 (helix) show similar dynamics despite the greater flexibility expected for a loop.[55,56] Solvent exposure seems to play a larger role in solvation than secondary structure as sites sharing the same secondary structures such as β-sheet sites (L7, W43, Y3, T16) and helix sites (F30, A24) show vastly different dynamics.

The dynamic Stokes shift of both A24 and W43, and to a much lesser extent T16, V21, and Y3, appear to undergo a blue shift at longer times (>1 ns). These blue shifts typically occur at long times when the overall fluorescence intensity has decayed to less than 20% of its initial value. Although the excited state of the chromophore is not expected to increase in energy along the solvation coordinate, a blue shift is possible if there are two or more subpopulations of the chromophore with different solvation dynamics and lifetimes. Given the correlation between fluorescence lifetime and the position of the probe (Figure 3), it is reasonable to consider the possibility that the blue shift is due to the presence of a small population of chromophores in a more protected environment than the fully exposed probe. Such a population would be expected to exhibit a smaller overall Stokes shift and possess a longer fluorescence lifetime. If this were the case, the dynamic Stokes shift at early times reflects the solvation dynamics of the dominant, short-lived population. As the intensity of the two populations becomes comparable, the emission maxima will appear to blue-shift and eventually the minor, long-lived component will dominate the solvation dynamics. A simple simulation is shown in Figure 7 and demonstrates that a blue shift can arise from two populations with different lifetimes and different solvation capacities. The origin of the minor emitting species is unknown, but plausible explanations include a small subpopulation of Aladan residues that are oriented into the protein core or the formation of GB1 aggregates which effectively bury the Aladan residue within a larger complex. Aggregation, while not observed in NMR studies of wild-type GB1,[38] may be more likely at the high protein concentrations used in these experiments ([GB1] ~ 0.42 mM). In addition, we cannot rule out the presence of minor impurities not apparent in the HPLC and LCMS analyses of the synthesized proteins, although the absence of these blue shifts from the proteins with buried Aladans (L7 and F30) would suggest that these shifts arise from some phenomenon at the protein surface. These blue shifts highlight the importance of measuring the solvation dynamics over the full lifetime of the probe when the data analysis involves normalization to the steady-state spectrum. Typically, ultrafast dynamic Stokes shift experiments in protein systems cover only a small fraction (< ~200 ps) of the fluorescence lifetime and either the final, time-resolved spectrum is normalized to the steady-state spectrum or the longest lifetime is fixed to a single value determined by other measurements.[17,25,26] Not only does this assume the absence of solvation dynamics on longer time scales and overestimate the ultrafast portion of the response, but it may also distort the dynamics of the Stokes shift over the observed window. Recently, Lu et al. noted a similar effect caused by the presence of multiple tryptophan rotamers in solution, each of which decays with a distinct fluorescence lifetime.[57] They propose a method to accurately separate the solvation dynamics

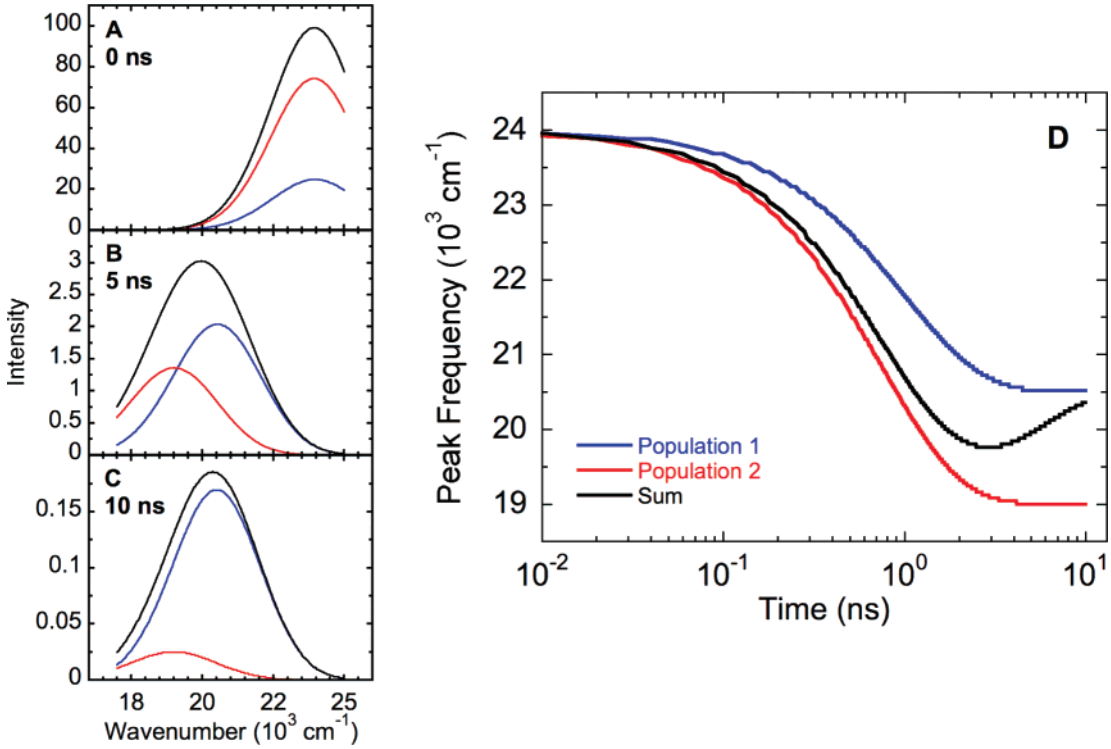

Figure 7. Simulation of the dynamic Stokes shift with two emitting populations illustrating a possible mechanism leading to a blue shift in the emission wavelength at long times. Population 1 (blue) has a lifetime of 2 ns and undergoes a peak shift of 3500 cm^{-1} with a time constant of 1 ns. Population 2 (red) has a lifetime of 1.25 ns and undergoes a peak shift of 5000 cm^{-1} with time constant 0.75 ns. The initial ratio of populations is 1:3. The emission spectra at 0 (A), 5 (B), and 10 ns (C) are shown for the two populations and their sum (black). (D) The resulting dynamic Stokes shift is shown (black) along with the dynamic Stokes shift of the individual populations.

from the apparent shift caused by differential population decay. Such an analysis is possible for tryptophan in solution, though an accurate separation of these effects is more complicated when $\tau_f \approx \tau_s$, as would be expected for tryptophan in a protein environment.

Conclusions

We have undertaken a comprehensive study of protein solvation response by introducing a fluorescent amino acid, Aladan, into seven unique sites in the interior and on the surface of the globular protein GB1. Probing the solvation dynamics with femtosecond resolution over the entire excited-state lifetime of the probe shows that solvation can occur on many time scales and that the dynamics depend on the location of the probe within the protein. All of the sites probed are capable of an initial ultrafast response (~80−140 fs), to varying degrees, and then exhibit differences at longer time scales. The exposed sites display dynamics that are qualitatively similar to the free fluorophore in solution. The partially buried sites show dynamics that extend to the time range of 100−1000 ps, while the buried sites exhibit dynamics consistent with slower, restricted motions of the surrounding amino acid residues and/or global protein motions that extend to ~10 ns. Solvent exposure rather than secondary structure had a more dominant role in dynamics. The method is based on the site-specific incorporation of a synthetic amino acid, so it can be extended to study a variety of sites within GB1 and other proteins of interest, even larger proteins by using protein semisynthesis strategies.[58] The small size of the GB1 protein and the time scales of the observed solvation responses are amenable to computer simulation techniques. Therefore, it may be possible through simulation to connect the specific structural solvation responses of the protein to the experimentally measured dynamics, and work toward this end is in progress.

Acknowledgment. This work was supported in part by grants from the NIH to S.G.B. (GM27738) and to Lily Y. Jan, UCSF (MH65334). The fluorescence upconversion facilities are supported by the Medical Free Electron Laser Program of the Air Force Office of Scientific Research (Grant F49620-00-1-0349). P.A. acknowledges financial support from the Fonds de recherche sur la nature et les technologies and the National Science and Engineering Research Council of Canada. We are grateful to Andrei A. Golosov and Martin Karplus for helpful discussions.

Supporting Information Available: Time-resolved fluorescence traces of Aladan-GB1's and NAAA. This material is available free of charge via the Internet at http://pubs.acs.org.

References and Notes

(1) Perutz, M. F. *Science* **1978**, *201*, 1187.
(2) Nakamura, H. *Q. Rev. Biophys.* **1996**, *29*, 1.
(3) Parson, W. W.; Chu, Z. T.; Warshel, A. *Biochim. Biophys. Acta* **1990**, *1017*, 251.
(4) Steffen, M. A.; Lao, K. Q.; Boxer, S. G. *Science* **1994**, *264*, 810.
(5) Okamura, M. Y.; Feher, G. *Annu. Rev. Biochem.* **1992**, *61*, 861.
(6) Hilvert, D. *Annu. Rev. Biochem.* **2000**, *69*, 751.
(7) Simonson, T.; Archontis, G.; Karplus, M. *J. Phys. Chem. B* **1997**, *101*, 8349.
(8) Aqvist, J.; Luzhkov, V. *Nature* **2000**, *404*, 881.
(9) Suydam, I. T.; Snow, C. D.; Pande, V. S.; Boxer, S. G. *Science* **2006**, *313*, 200.
(10) Horng, M. L.; Gardecki, J. A.; Papazyan, A.; Maroncelli, M. *J. Phys. Chem.* **1995**, *99*, 17311.
(11) Cohen, B. E.; McAnaney, T. B.; Park, E. S.; Jan, Y. N.; Boxer, S. G.; Jan, L. Y. *Science* **2002**, *296*, 1700.
(12) Pierce, D. W.; Boxer, S. G. *J. Phys. Chem.* **1992**, *96*, 5560.
(13) Sahu, K.; Mondal, S. K.; Ghosh, S.; Roy, D.; Bhattacharyya, K. *J. Chem. Phys.* **2006**, *124*, 124909.
(14) Lampa-Pastirk, S.; Warren, B. *J. Phys. Chem. B* **2004**, *108*, 16288.
(15) Golosov, A. A.; Karplus, M. *J. Phys. Chem. B* **2007**, *111*, 1482.
(16) Ware, W. R.; Chow, P.; Lee, S. K. *Chem. Phys. Lett.* **1968**, *2*, 356.

(17) Changenet-Barret, P.; Choma, C. T.; Gooding, E. F.; Degrado, W. F.; Hochstrasser, R. M. *J. Phys. Chem. B* **2000**, *104*, 9322.
(18) Jordanides, X. J.; Lang, M. J.; Song, X. Y.; Fleming, G. R. *J. Phys. Chem. B* **1999**, *103*, 7995.
(19) Pal, S. K.; Peon, J.; Zewail, A. H. *Proc. Natl. Acad. Sci. U.S.A.* **2002**, *99*, 15297.
(20) Zimmermann, J.; Oakman, E. L.; Thorpe, I. F.; Shi, X.; Abbyad, P.; Brooks, C. L., III; Boxer, S. G.; Romesberg, F. E. *Proc. Natl. Acad. Sci. U.S.A.* **2006**, *103*, 13722.
(21) Petushkov, V. N.; Van Stokkum, I. H. M.; Gobets, B.; Van Mourik, F.; Lee, J.; Van Grondelle, R.; Visser, A. J. W. G. *J. Phys. Chem. B* **2003**, *107*, 10934.
(22) Riter, R. R.; Edington, M. D.; Beck, W. F. *J. Phys. Chem.* **1996**, *100*, 14198.
(23) Homoelle, B. J.; Edington, M. D.; Diffey, W. M.; Beck, W. F. *J. Phys. Chem. B* **1998**, *102*, 3044.
(24) Guha, S.; Sahu, K.; Roy, D.; Mondal, S. K.; Roy, S.; Bhattacharyya, K. *Biochemistry* **2005**, *44*, 8940.
(25) Pal, S. K.; Peon, J.; Zewail, A. H. *Proc. Natl. Acad. Sci. U.S.A.* **2002**, *99*, 1763.
(26) Peon, J.; Pal, S. K.; Zewail, A. H. *Proc. Natl. Acad. Sci. U.S.A.* **2002**, *99*, 10964.
(27) Qiu, W.; Zhang, L.; Okobiah, O.; Yang, Y.; Wang, L.; Zhong, D.; Zewail, A. H. *J. Phys. Chem. B* **2006**, *110*, 10540.
(28) Toptygin, D.; Gronenborn, A. M.; Brand, L. *J. Phys. Chem. B* **2006**, *110*, 26292.
(29) Samanta, A.; Fessenden, R. W. *J. Phys. Chem. A* **2000**, *104*, 8972.
(30) Weber, G.; Farris, F. J. *Biochemistry* **1979**, *18*, 3075.
(31) Lobo, B. C.; Abelt, C. J. *J. Phys. Chem. A* **2003**, *107*, 10938.
(32) Viard, M.; Gallay, J.; Vincent, M.; Meyer, O.; Robert, B.; Paternostre, M. *Biophys. J.* **1997**, *73*, 2221.
(33) Vincent, M.; De Foresta, B.; Gallay, J. *Biophys. J.* **2005**, *88*, 4337.
(34) Parusel, A. B. J.; Nowak, W.; Grimme, S.; Kohler, G. *J. Phys. Chem. A* **1998**, *102*, 7149.
(35) Hiratsuka, T. *Biochemistry* **1998**, *37*, 7167.
(36) Krasnowska, E. K.; Gratton, E.; Parasassi, T. *Biophys. J.* **1998**, *74*, 1984.
(37) Rottenberg, H. *Biochemistry* **1992**, *31*, 9473.
(38) Gronenborn, A. M.; Filpula, D. R.; Essig, N. Z.; Achari, A.; Whitlow, M.; Wingfield, P. T.; Clore, G. M. *Science* **1991**, *253*, 657.
(39) Minor, D. L.; Kim, P. S. *Nature* **1994**, *371*, 264.
(40) Gardecki, J. A.; Maroncelli, M. *Appl. Spectrosc.* **1998**, *52*, 1179.
(41) Stanley, R. J.; Boxer, S. G. *J. Phys. Chem.* **1995**, *99*, 859.
(42) Chattoraj, M.; King, B. A.; Bublitz, G. U.; Boxer, S. G. *Proc. Natl. Acad. Sci. U.S.A.* **1996**, *93*, 8362.
(43) McAnaney, T. B.; Zeng, W.; Doe, C. F. E.; Bhanji, N.; Wakelin, S.; Pearson, D. S.; Abbyad, P.; Shi, X.; Boxer, S. G.; Bagshaw, C. R. *Biochemistry* **2005**, *44*, 5510.
(44) Steinbach, P. J.; Ionescu, R.; Matthews, C. R. *Biophys. J.* **2002**, *82*, 2244.
(45) Steinbach, P. J. *J. Chem. Inf. Comput. Sci.* **2002**, *42*, 1476.
(46) Sun, S. Y.; Heitz, M. P.; Perez, S. A.; Colon, L. A.; Bruckenstein, S.; Bright, F. V. *Appl. Spectrosc.* **1997**, *51*, 1316.
(47) Balter, A.; Nowak, W.; Pawelkiewicz, W.; Kowalczyk, A. *Chem. Phys. Lett.* **1988**, *143*, 565.
(48) Macgregor, R. B.; Weber, G. *Nature* **1986**, *319*, 70.
(49) Chakrabarti, A. *Biochem. Biophys. Res. Commun.* **1996**, *226*, 495.
(50) Hammarstrom, P.; Owenius, R.; Martensson, L. G.; Carlsson, U.; Lindgren, M. *Biophys. J.* **2001**, *80*, 2867.
(51) Tcherkasskaya, O.; Knutson, J. R.; Bowley, S. A.; Frank, M. K.; Gronenborn, A. M. *Biochemistry* **2000**, *39*, 11216.
(52) Kamal, J. K. A.; Xia, T. B.; Pal, S. K.; Zhao, L.; Zewail, A. H. *Chem. Phys. Lett.* **2004**, *387*, 209.
(53) Pal, S. K.; Peon, J.; Bagchi, B.; Zewail, A. H. *J. Phys. Chem. B* **2002**, *106*, 12376.
(54) Jimenez, R.; Fleming, G. R.; Kumar, P. V.; Maroncelli, M. *Nature* **1994**, *369*, 471.
(55) Kay, L. E.; Torchia, D. A.; Bax, A. *Biochemistry* **1989**, *28*, 8972.
(56) Idiyatullin, D.; Nesmelova, I.; Daragan, V. A.; Mayo, K. H. *Protein Sci.* **2003**, *12*, 914.
(57) Lu, W. Y.; Kim, J.; Qiu, W. H.; Zhong, D. P. *Chem. Phys. Lett.* **2004**, *388*, 120.
(58) Durek, T. T.; Becker, C. F. W. *Biomol. Eng.* **2005**, *22*, 153.
(59) Kuszewski, J.; Gronenborn, A. M.; Clore, G. M. *J. Am. Chem. Soc.* **1999**, *121*, 2337.